

# Effect of Nb addition on magnetic, structural and superconducting properties of (Bi, Pb)-2223 superconductors

O. Bilgili · K. Kocabaş

Received: 28 February 2014 / Accepted: 16 April 2014 / Published online: 28 April 2014  
© Springer Science+Business Media New York 2014

**Abstract** In this work, the effects of Nb<sub>2</sub>O<sub>5</sub> addition with different ratios on the structural and magnetic properties of Bi<sub>1.7-x</sub>Pb<sub>0.3</sub>Nb<sub>x</sub>Sr<sub>2</sub>Ca<sub>2</sub>Cu<sub>3</sub>O<sub>y</sub> ( $x = 0.00-0.20$ ) superconducting samples were investigated. (Bi, Pb)-2223 superconducting samples were prepared by conventional solid-state reaction method. The phase formation, phase fraction and lattice parameters were determined from X-ray powder diffraction (XRD) measurements, the microstructure, surface morphology analyses of the samples were carried out using scanning electron microscope (SEM). Additionally, ac susceptibility measurements were done in order to determine the critical current density ( $J_c$ ) and hole concentration ( $p$ ) of the samples. AC susceptibility measurements were done at various ac fields (ranging from 20 to 160 A/m) to understand the effect of Nb addition on magnetic properties of Bi<sub>1.7-x</sub>Pb<sub>0.3</sub>Nb<sub>x</sub>Sr<sub>2</sub>Ca<sub>2</sub>Cu<sub>3</sub>O<sub>y</sub> superconductor. Critical onset ( $T_c^{on}$ ) and loss peak temperatures ( $T_p$ ) were estimated from the ac susceptibility curves. It was observed from ac susceptibility measurements that the critical onset temperatures decreased from about 108–98 K with increasing Nb addition ( $x = 0.00-0.20$ ). The imaginary part of susceptibility was used to calculate the intergranular critical current density ( $J_c$ ) by means of the Bean's model. X-ray diffraction analysis revealed that the samples consisted of a mixture of Bi-2223 and Bi-2212 phases as the major constituents and non-superconducting phase Ca<sub>2</sub>PbO<sub>4</sub> as the minor. It was also shown from XRD measurements that volume fraction of high- $T_c$  phase decreases with increasing Nb addition up to  $x = 0.20$ . The sample with Nb addition of  $x = 0.20$  showed the highest volume fraction of Bi-2223 phase (86 %). When

Nb addition was increased, the surface morphology and grain connectivity are found to degrade, the grain sizes decrease and porosity of the samples were observed to increase from SEM images except the sample with  $x = 0.20$  Nb addition.

## 1 Introduction

Since the discovery of Bi-based superconductor ceramics, researchers have tried to improve their structural, magnetic and superconducting properties by using several techniques [1–7]. Superconductivity in the BSCCO system has been studied extensively because of their remarkable smaller power losses, high current and magnetic field carrying capacity and electronic properties. On the other hand, Bi-based superconductor application has major limitations such as intergrain weak links and weak flux pinning capability [8].

There have been several studies by substitution or addition of materials on the BSCCO system to improve the superconducting and magnetic properties [1–4]. Phase formation and physical properties in Bi-based system can be changed by substitution or addition of elements having different ionic radii and different bonding characters and also adjusting preparation conditions affect the properties in the system. The enhancement or destruction of the superconducting properties depends on the characteristics of the dopant in the crystal structure [9].

The general formula for Bi-based HTSCs can be stated as Bi<sub>2</sub>Sr<sub>2</sub>Ca<sub>n-1</sub>Cu<sub>n</sub>O<sub>2n+4</sub> in which  $n$  can take ( $n = 1, 2, 3$ ) values for the different number of Cu–O planes perpendicular to the  $c$ -axis. The phases are usually stated by the atomic ratio of the constituent elements of Bi:Sr:Ca:Cu as Bi-2201, Bi-2212, Bi-2223 for  $n = 1, 2, 3$  referring to the number of CuO<sub>2</sub> layers and incorporate the 20, 95 and 110 K superconducting phases, respectively [10].

O. Bilgili (✉) · K. Kocabaş  
Department of Physics, Dokuz Eylul University, 35160 Buca,  
Izmir, Turkey  
e-mail: ozlem.bilgili@deu.edu.tr

Some controversial works about the effect of Nb on the formation of Bi-2223 phase and other superconducting parameters of BSCCO are also reported in the literature. Mishra et al. reported that both the high- $T_c$  phase fraction and  $T_c$  decreases as the Nb concentration increases, being independent of the doping sites in a Pb-included BSCCO superconductor. Previous studies about the effects of Nb substitution on properties of BSCCO reported that  $T_c$  decreases with increasing Nb concentration in both Bi and Cu-sites. Some other studies have reported that Nb remains neutral in the superconducting lattice and have minimal effects on the properties [11]. In their study, Sozeri et al. reported that Nb addition enhances the high- $T_c$  2223 phase formation and improves the critical parameters  $T_c$  and  $J_c$ . It was also observed that Nb addition in very poor amount does not enhance the formation of Bi-2223, but improves intergrain connectivity which results in better superconducting properties of BSCCO systems [12]. Accordingly, critical current density is enhanced with Nb addition which is the most important feature [13]. Nasu et al. observed that  $T_c$  increased as Nb addition increased, resulting from the increase of the volume fraction of the high  $T_c$  phase. The microstructure is also influenced by Nb addition and grain size becomes smaller as Nb content becomes higher [14]. Similar to our study, Jafari et al. has found that Nb substitution increases the volume fraction of Bi-2223 phase and normal-state resistivity of Bi-based superconductors from XRD and R–T measurements. It was concluded that the Nb substitution decreases the flux pinning energy in line with our findings [15].

The ac susceptibility measurements provide useful information on bulk magnetic susceptibility which has a real ( $\chi'$ ) and imaginary part ( $\chi''$ ) and have been used in characterization of the high-temperature superconductors [16]. The sharp decrease in the real part below the critical temperature  $T_c$  is an indicator of diamagnetic shielding and the peak in the imaginary part represents the ac losses [17]. The real part of ac susceptibility, ( $\chi'$ ) show two drops as the temperature is lowered below onset of diamagnetic transition. The first sharp drop is due to the transition within grains and the second gradual change is due to the occurrence of superconducting coupling between grains. Under an external magnetic field, the imaginary part of ac susceptibility, ( $\chi''$ ) for the type II superconductors can show two peaks, if the external field is above a critical value. This phenomenon is believed to be due to intergrain and intragrain related effects, by using this, the intergrain and intragrain critical current density can be calculated [18, 19]. The main factors reducing the critical current density in HTSC are grain boundaries and poor flux pinning [20]. The low values of the grain boundary critical current densities in polycrystalline samples are a significant problem for large-current applications, for which the enhancements of critical current density is a key issue.

In this work, the effects of Nb addition on the microstructure and transport properties of  $\text{Bi}_{1.7-x}\text{Pb}_{0.3}\text{Nb}_x\text{Sr}_2\text{Ca}_2\text{Cu}_3\text{O}_y$  ceramics by using X-ray analysis (XRD), scanning electron microscopy (SEM) are reported. Magnetic and superconducting properties of Nb addition samples are also studied using ac susceptibility measurements. It is observed that the transition temperatures decrease as the Nb addition increases. Moreover, the surface morphology and grain connectivity are found to become poorer and the grain sizes of the samples are observed to decrease with increasing Nb addition up to  $x = 0.20$ .

## 2 Experimental details

Superconducting samples with chemical composition  $\text{Bi}_{1.7-x}\text{Pb}_{0.3}\text{Nb}_x\text{Sr}_2\text{Ca}_2\text{Cu}_3\text{O}_y$  ( $x = 0.00, 0.05, 0.10, 0.15, 0.20$ ) were prepared by solid state reaction method. The samples are labeled as Nb0, Nb1, Nb2, Nb3 and Nb4, respectively. Appropriate amounts of  $\text{Bi}_2\text{O}_3$ ,  $\text{PbO}$ ,  $\text{SrCO}_3$ ,  $\text{CaCO}_3$ ,  $\text{CuO}$  and  $\text{Nb}_2\text{O}_5$ , all of high purity (99.99 %) were mixed, ground and then calcinated at 800 °C for 20 h. The powder mixture was again calcined at 800 °C for 20 h in air after a second intermediate grinding. The final product after calcinations was grounded once more. Then, these powders were pressed under 450 MPa pressure using a press machine (Graseby Specac) to form them into pellets 13 mm in diameter and 1.5 mm thick. The prepared pellets were finally sintered at 845 °C for 120 h in air. The pellets were cooled in furnace up to room temperature after each cycle.

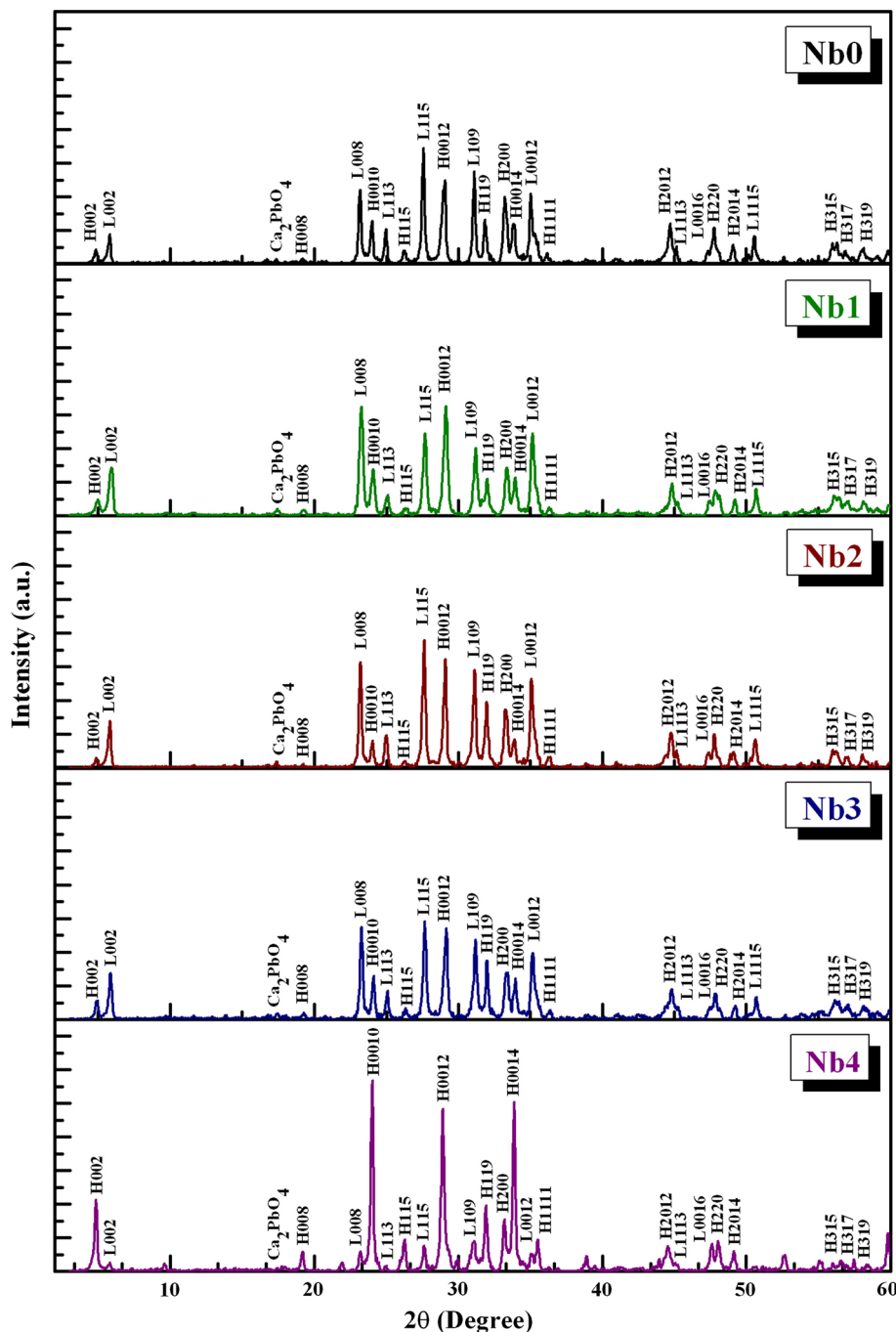
X-ray powder diffraction powder patterns were used to determine structure and fractions of high and low  $T_c$  phases. X-ray diffraction data were taken using  $\text{CuK}_\alpha$  radiation ( $\text{CuK}_\alpha$  radiation,  $\lambda = 0.154\ 06\ \text{nm}$ ) in the range  $2\theta = 3\text{--}60^\circ$ . The ac susceptibility measurements on the samples were performed using a home-made susceptometer and a lock-in amplifier (MODEL SR830 DSP Lock-in Amplifier). The sample was mounted such that its length was along the direction of the magnetic field. The temperature variation was enhanced using a closed cycle helium cryostat equipped with a temperature controller. AC field amplitudes of 20, 40, 80 and 160 A/m were used and frequency was fixed at 1,000 Hz. Susceptibility data taken from lock-in amplifier were recorded by using the Labview computer software.

## 3 Results and discussion

### 3.1 XRD studies

The results of XRD measurement patterns for samples Nb0, Nb1, Nb2, Nb3 and Nb4, respectively are shown in

**Fig. 1** XRD patterns of the  $\text{Bi}_{1.7-x}\text{Pb}_{0.3}\text{Nb}_x\text{Sr}_2\text{Ca}_2\text{Cu}_3\text{O}_y$  ( $x = 0.00, 0.05, 0.10, 0.15, 0.20$ ) samples



the Fig. 1. As seen from Fig. 1, the samples consist of a mixture of low- $T_c$  (2212), high- $T_c$  (2223) phases as the major constituents and non-superconducting phase  $\text{Ca}_2\text{PbO}_4$  as the minor. The (Bi, Pb)-2223 phase is called high- $T_c$  phase and their peaks are presented by H (hkl) and (Bi, Pb)-2212 phase is called low- $T_c$  phase and their peaks are presented by L (hkl). The peaks of  $\text{Ca}_2\text{PbO}_4$  phase are indicated by  $\text{Ca}_2\text{PbO}_4$ . The first peak H002, at  $2\theta \sim 4.7^\circ$ , corresponds to (Bi, Pb)-2223 phase whereas the second peak L002, at  $2\theta \sim 5.7^\circ$ , corresponds to (Bi, Pb)-2212

phase. The first peak intensity decreases while the second peak intensity increases with Nb addition up to  $x = 0.20$ .

Additionally, these results do not show the presence of  $\text{Nb}_2\text{O}_5$  in XRD patterns, that is, Nb may take a position in the interstitial or substitutional site thereby becoming part of the lattice. In our doped samples, Bi may be replaced with Nb atoms since the ionic radii of Nb (0.70 Å) is close to Bi (0.74 Å). When samples are calcined at a temperature higher than the melting point of  $\text{Bi}_2\text{O}_3$  (818 °C), some of the Bi atoms are lost, this results in the formation of the

**Table 1** Volume fractions of Bi-2223, Bi-2212 phases and grain size for samples Nb0, Nb1, Nb2, Nb3 and Nb4

Sample	Volume fraction (%)		Grain size (nm)
	Bi-2223	Bi-2212	
0.00	49.46	50.54	37
0.05	48.30	51.70	28
0.10	43.66	56.34	29
0.15	48.81	51.19	30
0.20	86.20	13.80	43

off-stoichiometric compound. Thus, we rather add Nb<sub>2</sub>O<sub>5</sub> than substituting it to the Bi site. Since Pb and Nb have similarities in size with Bi, different valency becomes an ideal candidate.

In this work, we have used all the peaks of Bi-2223 and Bi-2212 phases to estimate the volume fraction of the phases. The volume fractions of the Bi-2223 and Bi-2212 phases were determined from the peak intensities of the same particular reflections, using the following well-known expressions respectively;

$$\text{Bi} - (2223) \% = \frac{\sum I(2223)}{\sum I(2223) + I(2212)} \times 100$$

$$\text{Bi} - (2212) \% = \frac{\sum I(2212)}{\sum I(2223) + I(2212)} \times 100$$

I(2223) and I(2212) are the intensities of the (hkl) diffraction lines for Bi-(2223) and Bi-(2212) phases, respectively [21]. The volume fraction of the phases for all the samples is given in Table 1. As seen in the table, the volume fraction of Bi-2223 phase decrease from 49.46 to 43.66 for the samples having x = 0.00–0.10 and then increase to 86.20 for x = 0.20. The sample with x = 0.20 (Nb4) has shown the highest volume fraction of Bi-2223 phase among the others.

The lattice parameters (a, b, c) of the samples are calculated using the d values and (hkl) parameters by least-square-method and tabulated in Table 2. We observed that the lattice parameter c of the samples with Nb substitution decrease with increasing Nb content (Details are shown in Table 2).

**Table 2** Lattice parameters (a, b, c), volume of the orthorhombic cells in pure and Nb addition samples

Sample	Lattice parameters (Bi-2223 phase)				Lattice parameters (Bi-2212 phase)			
	a (Å)	b (Å)	c (Å)	V (Å <sup>3</sup> )	a (Å)	b (Å)	c (Å)	V (Å <sup>3</sup> )
0.00	5.405	5.405	37.298	1,089.625	5.3970	5.3970	30.807	897.3342
0.05	5.408	5.408	37.015	1,082.558	5.3946	5.3895	30.649	891.0951
0.10	5.399	5.413	37.130	1,085.116	5.3979	5.3979	30.685	894.0788
0.15	5.410	5.410	37.129	1,086.744	5.3946	5.3895	30.649	891.0951
0.20	5.400	5.420	37.154	1,087.423	5.3979	5.3979	30.685	894.0788

The values of grain sizes can be estimated from XRD measurements by using Scherrer Formula. The size of the grain in the polycrystalline materials has pronounced effects on many of the properties.

In Scherrer's equation

$$L = \frac{0.9\lambda}{t \cos\theta}$$

where L is the crystallite size in nm, λ is the wavelength of X-ray in nm, t is the FWHM (full width at half maximum) of the highest intensity peak and θ is the corresponding angle of the peak [22].

The grain sizes calculated from XRD patterns lies between 28 and 43 nm. The results of the calculations are tabulated in Table 1. As seen from the table, the average crystallite size of the superconducting samples increase with addition x = 0.20.

### 3.2 AC susceptibility measurements

Figure 2a–e displays the temperature dependencies of the real χ' (T) and imaginary χ'' (T) parts of ac susceptibility for the samples Nb0, Nb1 Nb2, Nb3 and Nb4 in the presence of different ac magnetic fields 20, 40, 80, 160 A/m with a frequency of 1,000 Hz, which are used for determination and characterization of the intragrain and inter-grain features of the high temperature superconductors.

The real component of ac susceptibility χ' (T) shows two significant drops when the temperature is decreased below onset of diamagnetic transition for superconductor samples.

The first sharp drop is due to the transition within grains and the second drop is due to the occurrence of the superconducting coupling between grains. In χ'-T curve, diamagnetic onset temperatures (T<sub>c</sub><sup>on</sup>) of the superconducting transition were observed to be about 108.46 K for Nb0, 105.85 K for Nb1, 103.80 K for Nb2, 105.43 K for Nb3, 98.18 K for Nb4 samples respectively and shown in Table 3. The superconducting transition temperature is shifted to lower temperatures with increasing Nb addition.

The imaginary component of ac susceptibility χ'' (T), generally displays two peaks with decreasing temperature below T<sub>c</sub>. Positions of these peaks are determined by the

**Fig. 2** Real and imaginary parts of ac susceptibility versus temperature plots for **a** Nb0, **b** Nb1, **c** Nb2, **d** Nb3 and **e** Nb4 in various ac field amplitudes at a frequency of 1 kHz

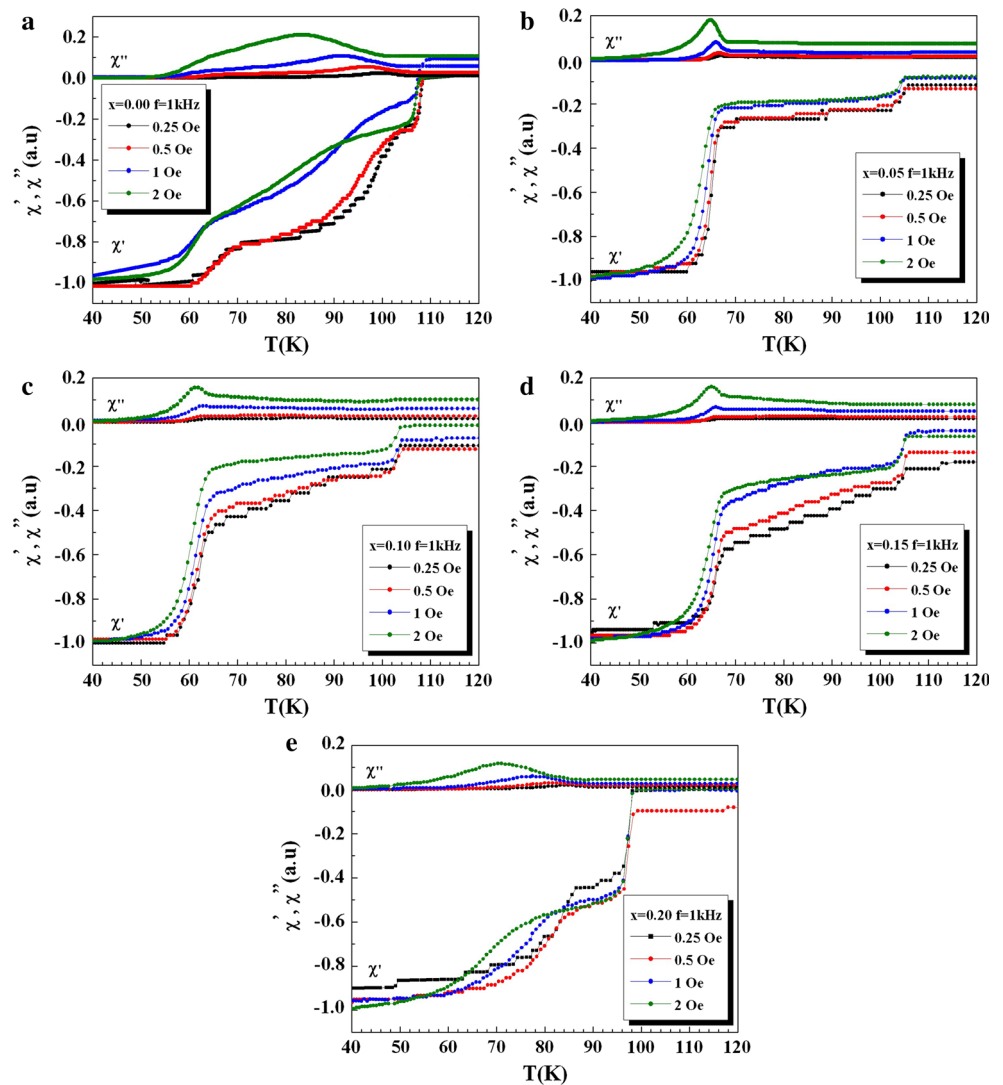


**Table 3**  $T_c^{on}$  and  $T_p$  temperature of Nb0, Nb1, Nb2, Nb3 and Nb4 samples at different field amplitudes

Sample	$T_c^{on}$ (K)	$T_p$ (K)			
		20 (A/m)	40 (A/m)	80 (A/m)	160 (A/m)
Nb0	108.46	99.756	96.636	91.429	83.401
Nb1	105.85	66.899	66.550	65.886	64.772
Nb2	103.80	63.304	62.376	62.082	61.121
Nb3	105.43	66.232	65.509	65.938	65.053
Nb4	98.180	84.847	81.619	77.017	71.287

strength of flux pinning. As the temperature increases, flux penetrates first into the intergrain region, which has a low pinning force and then into the intragrain material, which has a higher pinning force. At full flux penetration into the boundaries between the grains, the losses reach the maximum. Full flux penetration of the grains leads to the

appearance of intragrain loss peak, which occurs at a higher temperature due to the stronger flux pinning within the grains. The loss peak temperature ( $T_p$ ) shows the temperature where applied external magnetic field reaches center of the sample and the intensity of this peak is proportional to the energy loss within the intergrain area during the diamagnetic transition. The loss peak temperature ( $T_p$ ) represents the full flux penetration in the out of phase component of the samples, are noted to be about 99 (83) K for Nb0, 66 (64) K for Nb1, 63 (61) K for Nb2, 66 (65) K for Nb3, 84 (71) K for Nb4 at 20 (160) A/m ac field, respectively. It can clearly be seen from Fig. 2a–e that the imaginary part of ac susceptibility ( $\chi''$ ) depends on the applied ac field. The temperature where maximum peak observed in the imaginary part ( $T_p$ ) has decreased with increasing applied field to the sample.

It is also seen from Fig. 2a–e that as the field amplitude increases maximum peak temperature of imaginary part



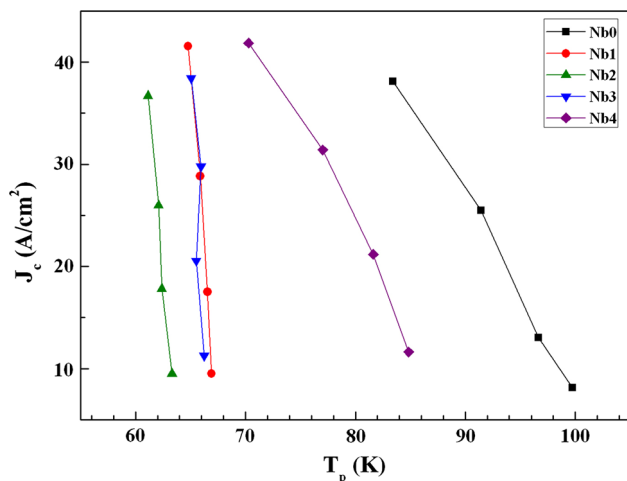


**Fig. 3**  $J_c$  versus  $T_p$  behavior for Nb0, Nb1, Nb2, Nb3 and Nb4 samples

( $T_p$ ) shifts to lower temperature and broadens. The amount of the shift as a function of the field amplitude is proportional to the magnitude or strength of the pinning force. The weaker the pinning effect, the larger is the shift in the maximum of  $\chi''$  and hence smaller the critical current. At the peak values of the imaginary part, ac field amplitude equals to the full flux penetration field,  $H_p$  [23]. We can estimate the intergranular critical current density as a function of temperature, by using the Bean Critical State Model. According to the Bean model [24], for the bar shaped sample the critical current density at the peak temperature  $T_p$ , can be written as the formula:

$$J(T_p) = H_p / \sqrt{ab}$$

where the cross section of the rectangular bar shaped sample is  $2a \times 2b$  [25, 26]. In Fig. 3, temperature variation of the critical current density for all samples plot is given. As can be seen, the increasing of Bi-2212 phase in the Bi-2223 system causes a decrease in the intergranular critical current density. Susceptibility behavior for samples Nb0, Nb1 Nb2, Nb3 shows that the Bi-2212 phase alter the weak link behavior of the Bi-2223 ceramics meaning the Bi-2212 phase resides in the grain boundaries and act as weak links in the Bi-2223 system.

In order to study the effect of Nb addition on the intergranular pinning force, the loss peak temperature dependence of the imaginary curves as a function of ac magnetic field ( $H_{ac}$ ) was investigated. Figure 4 shows the variation of peak temperature  $T_p$ , as a function of ac field amplitude,  $H_{ac}$  for samples Nb0, Nb1, Nb2, Nb3, Nb4. Figure 4 depicts the ac magnetic field dependence of loss peaks,  $T_p$ , for the samples produced. Muller critical state model proposes that  $T_p$  is linearly proportional to  $H_{ac}$  but

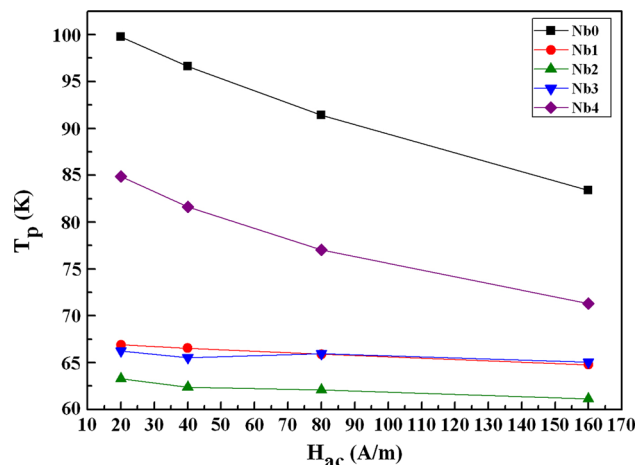


**Fig. 4** Intergranular peak temperature vs ac-magnetic field amplitude for Nb0, Nb1, Nb2, Nb3 and Nb4 samples

**Table 4** The extracted values of  $T_{p0}$  and  $U$  of the pure and Nb addition samples

Sample	$T_{p0}$ (K)	$U$ ( $\alpha_j(0)^{-1/2}$ )
Nb0	101.772	0.11888
Nb1	66.857	0.01387
Nb2	63.419	0.01352
Nb3	66.181	0.00664
Nb4	85.411	0.09179

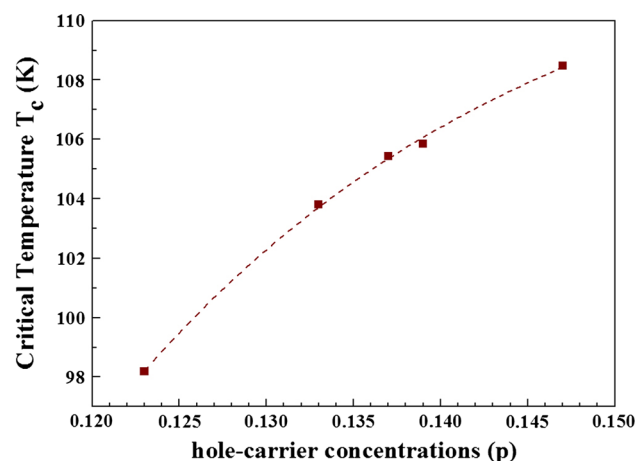


**Fig. 5** Variation of critical temperature versus hole-carrier concentrations

inversely proportional to the intergranular pinning force density:

$$T_p = T_{p0} - T_{p0} U^{1/2} H_{ac}$$

where  $U$  is

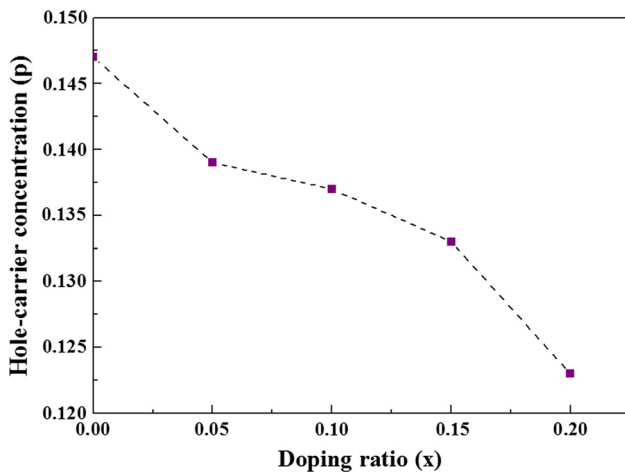


**Fig. 6** Variation of hole-carrier concentrations versus Nb Content for  $\text{Bi}_{1.7-x}\text{Pb}_{0.3}\text{Nb}_x\text{Sr}_2\text{Ca}_2\text{Cu}_3\text{O}_y$  ( $x = 0.00, 0.05, 0.10, 0.15, 0.20$ )

$$U = \frac{\mu_0 \mu_{\text{eff}}}{2a\alpha_J(0)}$$

Here,  $a$  is the length of the samples,  $\mu_{\text{eff}}$  is the effective permeability of the ceramic and  $\alpha_J(0)$  is the intergranular pinning force density [27]. As seen from Fig. 4, each set of data shows an excellent linear relationship between  $T_p$  and  $H_{ac}$ . The slope of each line is proportional to  $(\alpha_J(0))^{-1/2}$  and the vertical intercept of each line corresponds to the peak temperature,

$T_{p0}$ , at zero ac magnetic field amplitude. From least-squares fitting procedure by using the data  $T_{p0}$  and  $U$  were estimated for all samples and are depicted in Table 4. As seen from the table, the values of  $T_{p0}$  and  $U$  were found to decrease with increasing Nb addition up to  $x = 0.20$ . The decreasing trend in  $U$  means that the values of  $\alpha_J(0)$  increase with increase in the Nb addition because of the inverse ratio between  $U$  and  $\alpha_J(0)$ .  $T_{p0}$ ,  $U$  values has decreased with increasing Nb meaning  $\alpha_J(0)$  values increase with increasing Nb.

In conventional superconductors, the critical temperature increases monotonically with growth of charge carriers,  $T_c(p) \propto p$ . In cuprates, this dependence is non-monotonic. In most of hole-doped cuprates, the  $T_c(p)$  dependence has the bell-like shape.

$$T_c(p) = T_{c,\text{max}} \left[ 1 - 82.6(p - 0.16)^2 \right]$$

where  $T_{c,\text{max}}$  is the maximum critical temperature for a given compound. Superconductivity occurs within the limits,  $0.05 \leq p \leq 0.27$ , which vary slightly in various cuprates.

The hole-carrier concentrations per Cu ion,  $p$  are calculated by means of the following relation:

$$p = 0.16 - \left[ \left( 1 - \frac{T_c}{T_{c,\text{max}}} \right) / 82.6 \right]^{1/2}$$

where  $T_{c,\text{max}}$  is taken as 110 K for (Bi, Pb)-2223 phase [28]. As seen from the Fig. 5, the relationship between the

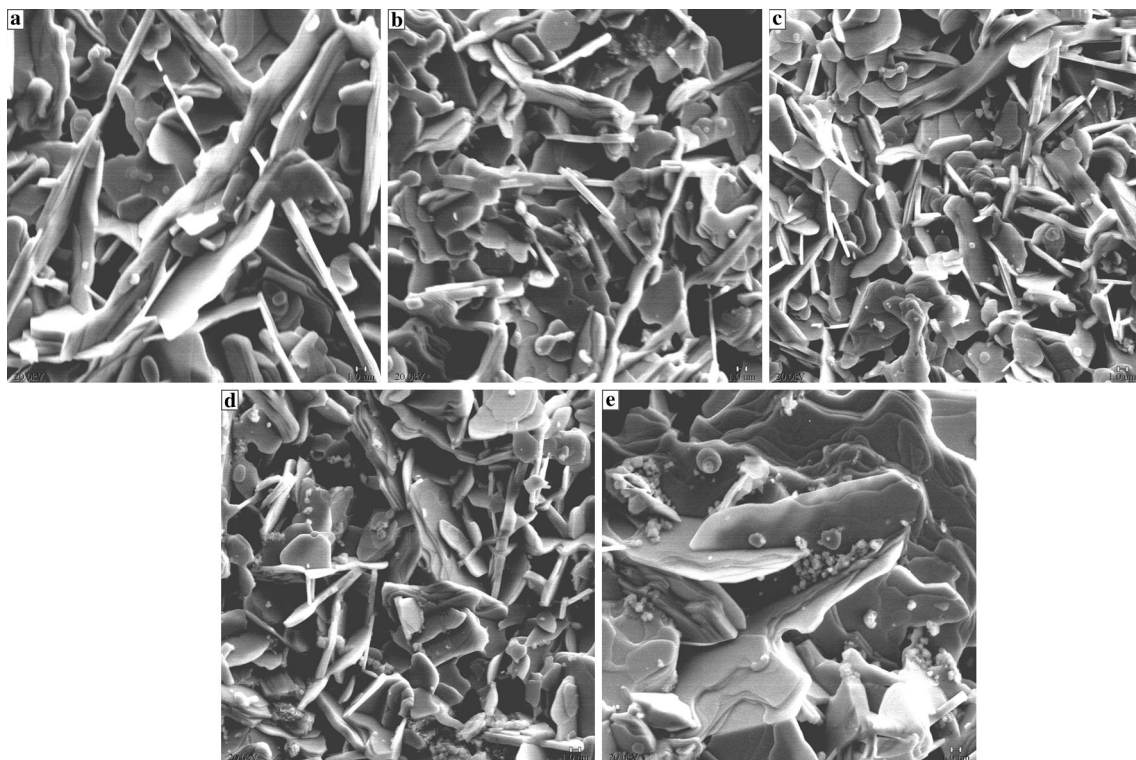


**Fig. 7** SEM micrographs of a Nb0, b Nb1, c Nb2, d Nb3 and e Nb4 samples

superconducting transition temperature  $T_c$  and hole-carrier concentration is parabolic. The Fig. 6 shows the decrease of hole-carrier concentration  $p$  with increasing Nb addition. The hole-carrier concentration of the pure sample is found to be greater than the others. Hole-carrier concentration was found to decrease from 0.147 to 0.123 with increasing Nb addition and decreasing  $T_c$ .

### 3.3 SEM analyses

The surface morphology images of the samples obtained are performed by Scanning Electron Microscopy (SEM). Figure 7a–e shows SEM images of the surface of the pure and Nb-added samples. The microstructures of all samples exhibit a common feature of plate-like grains and are randomly distributed. It is clearly seen from the figure that the surface morphology changes with Nb addition in the (Bi, Pb)-2223 system. The surface morphology, grain connectivity and average crystallite size are found to degrade with increasing the Nb addition. The grain morphology of the pure sample depicts the clear and flaky layers of large plate-like structure with random alignment distribution. On the other hand, the grain size and texturing of the doped samples up to  $x = 0.20$  are decreasing compared to the pure sample. With increasing Nb the grains started to degrade by random orientation, showing weak links between them. This increases the level of impurities, voids and porosity associated with the formation of smaller plate-like grains which belong to (Bi, Pb)-2212 phase. These results are consistent with that of XRD, which showed a decrease in the volume fraction of the (Bi, Pb)-2223 phase and an increase of (Bi, Pb)-2212 phase.

## 4 Conclusion

In this study, the role of Nb addition on the structural, magnetic and superconducting properties of (Bi, Pb)-2223 superconducting ceramics produced by the conventional solid-state reaction with Nb concentrations varying from  $x = 0.00$  to  $0.20$  is investigated via XRD, SEM and  $\chi$ -T measurements. AC magnetic susceptibility measurements showed degradation of the magnetic properties of the doped samples, i.e., the transition temperatures of the intragranular parts are significantly affected by the presence of Nb in Bi sites. From ac magnetic susceptibility measurement results, it was also seen that as Nb content increases, diamagnetic onset temperatures ( $T_c^{\text{on}}$ ) are observed to decrease from 108.46 to 98.18 K. Hole concentration of the samples, calculated by the results of ac magnetic susceptibility measurements, showed a decrease with increasing Nb concentration. The higher concentrations of Nb  $x = 0.20$  enhanced both the critical current density  $J_c$  and the volume

fraction of Bi-2223 phase compared to the pure sample. XRD analyses showed that the sample Nb with  $x = 0.20$  has the highest volume fraction of the Bi-2223 high- $T_c$  phase which is 86 %. The presence of  $\text{Nb}_2\text{O}_5$  was not observed in XRD patterns, indicating that Bi may be replaced with Nb atoms since the ionic radii of Nb are close to Bi. According to SEM results, the surface morphology and grain connectivity are noticed to degrade in the doped samples up to  $x = 0.20$ . It was also observed that Nb addition of  $x = 0.20$  improves intergrain connectivity which results in better superconducting properties of BSCCO system. The  $\text{Nb}_2\text{O}_5$  addition up to  $x = 0.20$  degrade the phase formation, grain connectivity, critical current density of (Bi, Pb)-2223 superconducting samples.

## References

- G. Yildirim, S. Bal, E. Yucel, M. Dogruer, M. Akdogan, A. Varilci, C. Terzioglu, *J. Supercond. Nov. Magn.* **25**, 381–390 (2012)
- J. Taghipour, H. Abbasi, H. Sedghi, *Phys. B* **405**, 1349–1352 (2010)
- P. Kameli, H. Salamati, M. Eslami, *Solid State Commun.* **137**, 30–35 (2006)
- O. Bilgili, Y. Selamet, K. Kocabas, *J. Supercond. Nov. Magn.* **21**, 439–449 (2008)
- K. Kocabas, S. Sakiroglu, M. Çiftçioglu, I. Ercan, H. Epik, O. Bilgili, *J. Supercond. Nov. Magn.* **22**, 749–754 (2009)
- M. Z. Shoushtari, A. Bahrami, M. Farbod, *Phys. Stat. Sol. c* **3**(9), 2994–2998 (2006)
- D. Yazıcı, B. Özçelik, M.E. Yakıncı, *J. Low Temp. Phys.* **163**, 370–379 (2011)
- M. Roumié, S. Marhaba, R. Awad, M. Kork, I. Hassan, R. Mawassi, *J. Supercond. Nov. Magn.* **2**(7), 143–153 (2014)
- A. Zelati, A. Amirabadizadeh, A. Kompany, H. Salamati, J. Somnier, *J. Supercond. Nov. Magn.* (2013). doi:10.1007/s10948-013-2475-y
- I.H. Gul, M.A. Rehman, M. Ali, A. Maqsood, *Phys. C* **432**, 71–80 (2005)
- D.R. Mishra, P.L. Upadhyay, R.G. Sharma, *Phys. C* **304**, 293–306 (1998)
- H. Sozeri, N. Ghazanfari, H. Özkan, A. Kılıç, **20**, 522–528 (2007)
- N. Ghazanfari, A. Kılıç, A. Gencer, H. Özkan, *Solid State Commun.* **144**, 210–214 (2007)
- H. Nasu, N. Kuriyama, K. Kamiya, *Japan. J. Appl. Phys.* **29**, 1415 (1990)
- M. Jafari, H. Sedghi, A. Esmaeili, *J. Supercond. Nov. Magn.* **26**, 3331–3338 (2013)
- S. Çelebi, *Phys. C* **316**, 251–256 (1999)
- A. Varilci, *Supercond. Sci. Technol.* **20**, 397–400 (2007)
- H. Salamati, P. Kameli, *Phys. C* **403**, 60–66 (2004)
- S. Çelebi, I. Karaca, E. Aksu, A. Gencer, *Phys. C* **309**, 131–137 (1998)
- A. Öztürk, I. Düzgün, S. Celebi, *J. Alloy. Compd.* **495**, 104–107 (2010)
- I.H. Gul, F. Amin, A.Z. Abbasi, M. Anis-ur-Rehman, A. Maqsood, *Phys. C* **449**, 139–147 (2006)
- M. Anis-ur-Rehman, *J. Alloy. Compd.* **469**, 66–72 (2009)
- C. Terzioglu, D. Yegen, M. Yılmazlar, O. Gorur, M. Akdogan, A. Varilci, *J. Mater. Sci.* **42**, 4636–4641 (2007)



24. C.P. Bean, *C.P. Rev. Mod. Phys.* **36**, 31 (1964)
25. P. Kameli, H. Salamati, I. Abdolhosseini, *J. Alloy. Compd.* **458**, 61–65 (2008)
26. V. Mihalache, I.G. Deac, A.V. Pop, L. Miu, *Curr. Appl. Phys.* **11**, 1010–1014 (2011)
27. G. Yildirim, Y. Zalaoglu, M. Akdogan, S.P. Altintas, A. Varilci, C. Terzioglu, *J. Supercond. Nov. Magn.* **24**, 2153–2159 (2011)
28. M.R. Persland, J.L. Tallon, R.G. Buckley, R.S. Liu, N.E. Flower, *Phys. C* **176**, 95–105 (1991)